# A Simple and Practical Underlay Scheme for Short-range Secondary Communication

Mohamed Salah Ibrahim, *Member, IEEE,* Paris A. Karakasis, *Student Member, IEEE,* and Nicholas D. Sidiropoulos, *Fellow, IEEE*

***Abstract*—The unprecedented growth in wireless Internet-of-Things and WiFi devices has renewed interest in mechanisms for efficient spectrum reuse. Existing schemes require some level of primary-secondary coordination, cross-channel state estimation and tracking, or activity detection – which complicate implementation. For low-power short-range secondary communication, the main impediment is strong and time-varying (e.g., intermittent) interference from the primary system. This paper proposes a practical underlay scheme that permits reliable secondary communication in this regime. The secondary transmitter merely has to send its signal twice, at very low power - a few dBs above the noise floor, but far below the primary's interference. Exploiting the repetition structure, reliable and computationally efficient recovery of the secondary signal is possible via canonical correlation analysis (CCA). Experiments using a software radio testbed reveal that, for a secondary user with only two receive antennas, reliable detection of the secondary signal is possible for signal to interference plus noise ratio (SINR) in the range of -20 to -40 dB. The approach works with unknown time-varying channels, digital or analog modulation, it is immune to carrier frequency offset, and, as a side-benefit, it provides means for accurate synchronization of the secondary user even at very low SINR.**

***Index Terms*—Spectrum sharing, dynamic spectrum access, underlay communication, canonical correlation analysis, cognitive radio networks, unsupervised detection, synchronization.**

## I. Introduction

The rapidly growing demand for wireless connectivity from 5G+ to Internet of Things (IoT) and WiFi-enabled devices has brought renewed interest and impetus behind dynamic spectrum sharing [2]–[4]. Even with millimeter-wave (mmWave) technology, the propagation loss in the 28 GHz - 300 GHz bands is much higher than in the sub-6 GHz bands [5], making the latter better-suited for various wireless systems. The premium placed on sub-6 GHz bands together with the need to protect scientific uses in the mmWave bands are driving the renewed interest in spectrum sharing and dynamic spectrum access (DSA).

DSA techniques are designed to improve spectrum utilization by allowing secondary unlicensed users to take advantage of ephemeral transmission opportunities in space, time, or frequency [6]–[8] – a capability often referred to as *cognitive radio*. Currently, there are three widely used DSA techniques for cognitive radio networks (CRN): interweaving, overlay, and underlay [2]. In the interweaving mode, the secondary users search the band for spectrum holes (vacant sub-bands) which represent secondary transmission opportunities. The overlay paradigm requires tight coordination between the primary and secondary users, which complicates implementation. Relative to the interweaving and overlay modalities, underlay spectrum sharing is appealing in terms of its prioritization of the licensed / legacy users, practical feasibility, and its relative simplicity – there is no need for continuous spectrum sensing or tight coordination with the primary system.

There is a plethora of works on DSA and cognitive radio, spanning two decades of research ranging from spectrum sensing [9], [10] and channel gain "cartography" [11] to different spectrum sharing modalities [12]–[24]. A common assumption in those works is that the signal to interference plus noise ratio (SINR) at the secondary receiver can be made high enough to enable reliable decoding. In practice, this is hard to ensure if the primary transmitter is powerful (e.g., a TV or radio station) while the secondary is power-limited (e.g., a WiFi or IoT device). Furthermore, many of these works are relying on assumptions that are hard to meet in practice – such as the availability of cross-channel knowledge at the secondary users.

Few spectrum underlay works have attempted to circumvent the need for such assumptions. One interesting recent example is [25], where the authors proposed a nice semi-blind beamforming-based underlay spectrum sharing approach, which allows the secondary users to access the spectrum while minimally affecting the primary network performance, without requiring any channel knowledge at the secondary network. However, the proposed method in [25] still requires i) the primary communication to be bidirectional (which does not hold for legacy radio/TV broadcast, or scientific uses); ii) the flow direction of primary traffic to be predictable; iii) effectively time-invariant channels from/to the primary users; and iv) training pilots for designing the beamformer at the secondary receiver. These are still restrictive assumptions. In particular, the reverse transmission of the primary user needs to be synchronized with the forward of the

Manuscript received August 22, 2021; revised February 26, 2022; accepted June 1, 2022. This work was supported in part by the National Science Foundation (NSF) under Grants ECCS-1807660, ECCS-1852831, and ECCS-2118002. This article was presented in part at the IEEE International Conference on Acoustics, Speech, and Signal Processing (ICASSP), Toronto, Canada, June 2021 [1]. The associate editor coordinating the review of this article and approving it for publication was Prof. Min Sheng. Mohamed Salah Ibrahim and Paris A. Karakasis contributed equally to this work. (Corresponding author: Mohamed Salah Ibrahim.)

Mohamed Salah Ibrahim was with the Department of Electrical and Computer Engineering, University of Virginia, Charlottesville, VA, 22904 USA (e-mail: salah@virginia.edu); he is now with Interdigital Communications, Conshohocken, PA 19428, USA.

Paris A. Karakasis, and Nicholas D. Sidiropoulos are with the Department of Electrical and Computer Engineering, University of Virginia, Charlottesville, VA, 22904 USA (email: karakasis@virginia.edu, nikos@virginia.edu).

secondary, and vice versa, so the secondary users need to track which node is transmitting in the primary network.

Is it possible to design an underlay strategy that enables reliable decoding at very low SINR and modest SNR at the secondary receiver, without noticeable increase of the noise floor at the primary receiver? Is it possible to do this seamlessly, without any coordination between the primary (legacy / incumbent) and the secondary user?

The answer is, surprisingly, affirmative. This paper proposes a secondary transmission protocol that operates at very low power yet allows reliable secondary communication without requiring any channel knowledge or coordination with the primary system. The key idea is that the secondary user sends its signal twice, each time at very low power. Assuming that the secondary receiver employs at least two receive antennas, the proposed transmission protocol allows the secondary receiver to create two "views" of the signal space that only share the secondary signal – the interference from the primary network is potentially very strong, but different in the two views. Invoking canonical correlation analysis (CCA) on these two views, the secondary receiver can reliably decode its intended signal under very strong interference from the primary user.

Transmitting the same signal twice can be viewed as repetition coding [26], or as elementary direct-sequence spreading [27], [28] with spreading gain equal to two. Our approach is fundamentally different from these classical techniques *in the way that this controlled redundancy is exploited at the receiver* (i.e., on the "decoding" side), where we leverage the unique strengths of CCA. CCA is a well-known statistical learning tool that seeks to find linear combinations of two random vectors such that the resulting pair of random variables is maximally correlated [29]. In recent work [30], we came up with a new and broadly useful algebraic interpretation of CCA as a method that identifies a common (shared) subspace between two signal views, even under strong interference from individual (per-view) components. CCA has found many other applications in signal processing and wireless communications, including direction-of-arrival estimation [31], equalization [32], radar [33], [34], blind source separation [35], [36], and more recently cell-edge user detection [37], [38], and multi-view learning [39]–[41], to name a few.

Our contributions and the merits of this paper can be summarized as follows:

- We propose a novel secondary underlay framework that enables seamless primary-secondary coexistence – there is no need for coordination between the two. Assuming that the secondary receiver is equipped with two receive antennas and down-conversion chains, simple repetition of the secondary signal coupled with CCA processing at the secondary receiver can recover the secondary transmission even at very low SINR. This claim is rigorously backed by identifiability and new theoretical performance analysis in the noisy case.
- The approach is data-driven and unsupervised in that it directly recovers the secondary information signal (up to complex scaling), without requiring channel state information or primary signal recovery and cancellation. It even works with analog modulation of the primary and/or the secondary signal.
- Time-varying channels for the primary and the secondary user can be naturally accommodated, provided that the channel coherence time is greater than half the secondary transmission frame length (comprising a transmitted packet and its repetition – and the packet length is up to our control and can be fairly short).
- From a computational point of view, what is required is the computation and inversion of small correlation matrices, and then a principal eigenvector computation, which can be done using e.g., the power method. Hence, the approach is attractive for practical implementation.
- The approach is immune to carrier frequency offset, which can be compensated after the secondary symbol sequence is extracted using CCA. Furthermore, exploiting the repetition structure and CCA, we develop a matching synchronization algorithm that identifies the correct timing of the secondary transmission frames even at very low SINR in an unsupervised manner – i.e., without using any pilot symbols, only exploiting the structured redundancy introduced by repetition. These side-benefits are very fortunate, for otherwise synchronization is a very difficult problem at very low SINR without very long pilot sequences for acquisition.
- Last but not least, in order to demonstrate the practical feasibility and merits of our approach we have built and tested a prototype using software defined radios, where both the secondary and primary users were realized using USRP-2920 radios. We conducted multiple experiments to evaluate the performance of the proposed underlay CCA approach under realistic conditions. Our laboratory experiments verified that the proposed approach can reliably recover a secondary user signal that is buried under strong interference from the primary system (SINR as low as -40 dB), and that it approaches the attainable detection performance in the interference-free regime (where the primary user is idle). Further, simulations are also provided to show the impact of the number of secondary receive antennas, higher order modulation and different fading scenarios, on the performance of the proposed method.

A preliminary version of part of the results in this paper has been accepted for presentation at the IEEE International Conference on Acoustics, Speech, and Signal Processing (ICASSP) 2021 [1]. Relative to the conference paper, this journal version includes i) a generalization of the synchronous model in [1] to the practical setup where the two transmitters are not synchronized; ii) comprehensive solution of practical synchronization issues at the secondary receiver, including a low-complexity algorithm; iii) theoretical performance analysis; iv) additional simulations and baselines; and v) the design and execution of extensive laboratory experiments, and discussion of associated insights obtained using the software radio testbed we developed for this purpose.

The rest of this paper is organized as follows. After briefly reviewing CCA in Section II, Section III presents the system

model and highlights the major limitations of the prior art in terms of secondary underlay schemes. The proposed secondary transmission protocol is described in Section IV, while the proposed detector is presented in Section V. Section VI explains how to resolve synchronization issues at the secondary receiver. Experimental results are provided in Section VII, and conclusions are drawn in Section VIII.

## II. Overview of CCA

Consider two data sets $\mathbf{Y}_1 = [\mathbf{y}_1^{(1)}, \cdots, \mathbf{y}_1^{(N)}] \in \mathbb{C}^{M_1 \times N}$ and $\mathbf{Y}_2 = [\mathbf{y}_2^{(1)}, \cdots, \mathbf{y}_2^{(N)}] \in \mathbb{C}^{M_2 \times N}$, where $\mathbf{y}_\ell^{(n)}$ represents the $n$-th realization of the random vector $\mathbf{y}_\ell$ associated with the $\ell$-th view, $\ell \in \{1, 2\}$. We assume without loss of generality that all the data vectors $\{\mathbf{y}_\ell^{(n)}\}_{n=1}^N$ in each view are zero-mean, otherwise the sample mean can be subtracted as a pre-processing step.

In its simplest form, CCA aims to find two linear combinations of the elements of random vectors $\mathbf{y}_1$ and $\mathbf{y}_2$, $z_1 = \mathbf{q}_1^H \mathbf{y}_1$ and $z_2 = \mathbf{q}_2^H \mathbf{y}_2$, respectively, such that the two derived random variables $z_1$ and $z_2$ are maximally correlated, where $(\cdot)^H$ denotes conjugate transpose. In that sense, CCA seeks to find a "latent" component that is common between the two random vectors. From an optimization perspective, the CCA problem can be posed as [29], [42],

$$\max_{\mathbf{q}_1, \mathbf{q}_2} \ \mathrm{Re}\left\{\mathbf{q}_1^H \mathbf{Y}_1 \mathbf{Y}_2^H \mathbf{q}_2\right\} \tag{1a}$$

$$\text{s.t.} \quad \mathbf{q}_\ell^H \mathbf{Y}_\ell \mathbf{Y}_\ell^H \mathbf{q}_\ell = 1, \quad \ell \in \{1, 2\}, \tag{1b}$$

where $\mathrm{Re}\{\cdot\}$ extracts the real part of its argument. Notice that the scaling constraints serve to exclude the trivial (and meaningless) all-zero solution. An appealing feature of CCA that renders it suitable for practical implementation is that (1) admits an algebraic solution via eigendecomposition [42]. In particular, the optimal canonical vectors can be obtained via first solving the following generalized eigenvalue problem to obtain $\mathbf{q}_1^\star$ and $\lambda^\star$,

$$\mathbf{R}_{12} \mathbf{R}_2^{-1} \mathbf{R}_{21} \mathbf{q}_1 = \lambda \mathbf{R}_1 \mathbf{q}_1. \tag{2}$$

where $\mathbf{R}_i = \frac{1}{N} \mathbf{Y}_i \mathbf{Y}_i^H$ is the sample auto-covariance of the random vector $\mathbf{y}_i$, and $\mathbf{R}_{ij} := \frac{1}{N} \mathbf{Y}_i \mathbf{Y}_j^H$ is the sample cross-covariance of the two random vectors $\mathbf{y}_i$ and $\mathbf{y}_j$, respectively, for $i, j = 1, 2$ and $i \neq j$. Further, it can be easily verified that the term $\lambda^\star$ represents the square of the correlation coefficient, $\rho(\mathbf{q}_1^\star, \mathbf{q}_2^\star)$, associated with the optimal canonical pair $\mathbf{q}_1^\star$ and $\mathbf{q}_2^\star$, where

$$\rho(\mathbf{q}_1^\star, \mathbf{q}_2^\star) = \mathrm{Re}\{\mathbf{q}_1^{\star H} \mathbf{Y}_1 \mathbf{Y}_2^H \mathbf{q}_2^\star\}. \tag{3}$$

Once the optimal $\mathbf{q}_1^\star$ and $\lambda^\star$ are obtained from solving (2), the optimal $\mathbf{q}_2^\star$ can be obtained via direct substitution in the following

$$\mathbf{q}_2^* = \frac{1}{\sqrt{\lambda^*}} \mathbf{R}_2^{-1} \mathbf{R}_{21} \mathbf{q}_1^*. \tag{4}$$

A more intuitive formulation of (1) (that also happens to be more convenient for our purposes) is to minimize the distance between the linear projections of $\mathbf{Y}_1$ and $\mathbf{Y}_2$ on $\mathbf{q}_1$ and $\mathbf{q}_2$, respectively. That is [42], [43],

$$\min_{\mathbf{q}_1, \mathbf{q}_2} \ \|\mathbf{Y}_1^H \mathbf{q}_1 - \mathbf{Y}_2^H \mathbf{q}_2\|_2^2 \tag{5a}$$

$$\text{s.t.} \quad \mathbf{q}_\ell^H \mathbf{Y}_\ell \mathbf{Y}_\ell^H \mathbf{q}_\ell = 1, \quad \ell = \{1, 2\} \tag{5b}$$

Expanding the cost of problem (5) and using the constraints, the equivalence between (1) and (5) can be easily verified. Throughout this work, we will focus on the distance minimization formulation of CCA.

In what follows, we will see how judicious design of the secondary signaling protocol can be used to leverage the power of CCA to enable simultaneous and fully independent operation of two coexisting systems without affecting each other's performance.

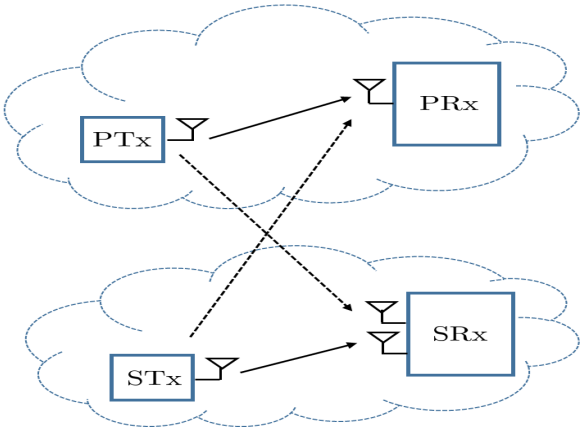


Fig. 1: System Model

## III. System Model

Consider an underlay cognitive radio network comprising a single-antenna secondary transmitter (STx) communicating with a secondary receiver (SRx) equipped with $M_s \geq 2$ antennas, in the presence of a single-antenna primary transmitter (PTx) and primary receiver (PRx) with $M_p \geq 1$ antennas, as shown in Fig. 1. Multiple secondary and primary users can also be accommodated as we will explain later. Let $\mathbf{h}_s \in \mathbb{C}^{M_s}$, $\mathbf{h}_{ps} \in \mathbb{C}^{M_s}$, $\mathbf{h}_{sp} \in \mathbb{C}^{M_p}$ and $\mathbf{h}_p \in \mathbb{C}^{M_p}$ be the channel response between the STx and SRx, PTx and SRx, STx and PRx, and PTx and PRx, respectively, defined as

$$\begin{aligned} \mathbf{h}_s &= \sqrt{\sigma_{ss}}\, \mathbf{g}_s, \quad \mathbf{h}_{ps} = \sqrt{\sigma_{ps}}\, \mathbf{g}_{ps}, \\ \mathbf{h}_p &= \sqrt{\sigma_p}\, \mathbf{g}_p, \quad \mathbf{h}_{sp} = \sqrt{\sigma_{sp}}\, \mathbf{g}_{sp}, \end{aligned} \tag{6}$$

where $\mathbf{g}_s$, $\mathbf{g}_{ps}$, $\mathbf{g}_{sp}$, and $\mathbf{g}_p$ are the respective small-scale fading vectors, while the terms $\sigma_{ss}$, $\sigma_{ps}$, $\sigma_{sp}$, and $\sigma_p$ are the corresponding large scale fading coefficients with values dependent on the propagation distance and environment.

Unlike prior works [15]–[19] that require estimates of the cross channels $\mathbf{h}_{ps}$ and/or $\mathbf{h}_{sp}$ at the secondary receiver and the secondary transmitter, respectively, this paper considers a practical setting where the secondary users have no knowledge about any channel state information in the network.

### A. Signal Model

We assume that the primary users transmission is done over a narrowband channel of bandwidth $B$ Hz. For simplicity of exposition, we assume that both users are employing QPSK modulation, but other types of modulation can be accommodated. The basic approach we propose to recover the secondary signal is modulation-agnostic, and does not assume anything about the primary signal's modulation, which can even be analog.

Let $\mathbf{x}_p \in \mathbb{C}^N$ and $\mathbf{x}_s \in \mathbb{C}^N$ denote the digitally-modulated transmitted signal by the primary and secondary user, respectively, where $|\mathbf{x}_p(n)|^2 = 1$ and $|\mathbf{x}_s(n)|^2 = 1$ for $n \in [N] := \{1, \cdots, N\}$. In writing down the discrete-time baseband-equivalent model, we shall assume, for simplicity of exposition, that the primary and secondary signals are synchronized at the symbol level – otherwise writing down the model is cumbersome. However, such an assumption is not required for our approach to work, and we shall later present an algorithm that can lock on the secondary user signal at the SRx. All our laboratory experiments are concerned with this asynchronous setup.

The discrete-time synchronous baseband-equivalent model of the received signal, $\mathbf{Y}_s \in \mathbb{C}^{M_s \times N}$, at the secondary receiver is given by

$$\mathbf{Y}_s = \sqrt{\alpha_s}\mathbf{h}_s\mathbf{x}_s^T + \sqrt{\alpha_p}\mathbf{h}_{ps}\mathbf{x}_p^T + \mathbf{W}_s, \tag{7}$$

where $\alpha_s$ and $\alpha_p$ are the transmit power of the STx and PTx, respectively. The term $\mathbf{W}_s \in \mathbb{C}^{M_s \times N}$ represents noise and it contains independent identically (i.i.d) distributed elements with each entry drawn from a complex Gaussian distribution with zero mean and variance $\sigma_s^2$. Similarly, the received signal at the primary receiver, $\mathbf{Y}_p \in \mathbb{C}^{M_p \times N}$, is given by

$$\mathbf{Y}_p = \sqrt{\alpha_s}\mathbf{h}_{sp}\mathbf{x}_s^T + \sqrt{\alpha_p}\mathbf{h}_p\mathbf{x}_p^T + \mathbf{W}_p, \tag{8}$$

where $\mathbf{W}_p \in \mathbb{C}^{M_p \times N}$ is the noise term at the primary receiver with i.i.d entries drawn from a complex Gaussian distribution with zero mean and variance $\sigma_p^2$.

### B. Our Goal

The goal of this work is to show that, in the absence of channel state information at the STx/SRx and without any coordination between the primary and secondary users, seamless secondary underlay communication is possible without affecting the primary network performance. To do this, we will first present a simple secondary transmission protocol together with a data-driven (unsupervised learning-based) approach that allow i) the STx to transmit its signal at very low power so that it does not affect the detection performance at the PRx, thereby keeping the resulting interference close to the PRx noise floor (the PRx can reliably decode its signal even with one receive antenna), and ii) the SRx to reliably decode its intended signal at significantly low SINR (e.g., -40 dB).

## IV. Secondary Transmission Protocol

In this section, we will present a simple transmission protocol that will assist the secondary transmitter to reliably communicate with its receiver over the same channel occupied by the primary network, and without degrading the primary user's performance.

The secondary transmission scheme is described as follows. If a secondary user desires to transmit in a channel occupied by a primary user, it simply transmits the same sequence twice at very low power – enough to be received above the thermal noise floor at the SRx, but far below what is required to be directly decoded in the face of possibly overwhelming interference by the PTx. The repetition of the secondary user's sequence can happen at the symbol or block level; we assume block-repetition for simplicity of exposition. To do this, we write $\mathbf{x}_s$ as two back-to-back repeated blocks, i.e., $\mathbf{x}_s = [\mathbf{s}^T\ \mathbf{s}^T]^T$, where $\mathbf{s} \in \mathbb{C}^{N/2}$ is the transmitted QPSK symbols by the secondary user over each block. Partitioning $\mathbf{x}_p = [\mathbf{p}_1^T\, \mathbf{p}_2^T]^T$ in two blocks for convenience, the received signal at the secondary receiver in (7) can be rewritten as

$$\mathbf{Y}_s = \mathbf{H}_s \begin{bmatrix} \mathbf{s} & \mathbf{p}_1 \\ \mathbf{s} & \mathbf{p}_2 \end{bmatrix}^T + \mathbf{W}_s, \tag{9}$$

where $\mathbf{H}_s$ is an $M_s \times 2$ matrix that holds on the first column the channel vector containing the channel coefficients between the STx and SRx, $\mathbf{h}_s$, and on the second column the channel from the PTx to the SRx, $\mathbf{h}_{ps}$. Notice that the transmit power terms of both the STx and PTx have been absorbed in the respective channel vectors, for brevity.

As noted earlier, the proposed transmission scheme can be interpreted as repetition coding [26], or equivalently as direct-sequence spreading of the secondary user's transmission with spreading gain equal to two [27]. Treating this situation as CDMA or as an error control problem will not work, because the primary user dominates the received signal, and small spreading / coding gains cannot make up for the large power difference between the secondary and primary user. CDMA performance is known to suffer from the so-called *near-far* problem which is clearly the case for the setup considered herein.

We will next present a low-complexity learning-based approach that allows the SRx to reliably decode its intended signal, $\mathbf{s}$, even if the received SINR is significantly low.

## V. Secondary Signal Detection via CCA

By exploiting the repetition structure, the SRx can split $\mathbf{Y}_s$ and $\mathbf{W}_s$ into two blocks, $\mathbf{Y}_s = [\mathbf{Y}_1\ \mathbf{Y}_2]$, and $\mathbf{W}_s = [\mathbf{W}_1\ \mathbf{W}_2]$, for which we have

$$\mathbf{Y}_1 = \mathbf{H}_s\ [\mathbf{s}\ \mathbf{p}_1]^T + \mathbf{W}_1, \tag{10}$$

$$\mathbf{Y}_2 = \mathbf{H}_s\ [\mathbf{s}\ \mathbf{p}_2]^T + \mathbf{W}_2 \tag{11}$$

Now, given the two signal views in (10), CCA will be invoked to show that reliable detection of the secondary signal, $\mathbf{s}$, is possible even at low SINR. To see how we can utilize CCA to identify the secondary signal, $\mathbf{s}$, from $\mathbf{Y}_1 \in \mathbb{C}^{M_s \times N/2}$

and $\mathbf{Y}_2 \in \mathbb{C}^{M_s \times N/2}$, we will use the so-called *maximum variance* (MAX-VAR) formulation of CCA [42]. That is

$$\min_{\mathbf{g},\mathbf{q}_1,\mathbf{q}_2} \sum_{\ell=1}^{2} \|\mathbf{Y}_\ell^T \mathbf{q}_\ell - \mathbf{g}\|_2^2, \tag{12a}$$

$$\text{s.t.} \quad \|\mathbf{g}\|_2^2 = 1. \tag{12b}$$

The MAX-VAR formulation is equivalent to the distance minimization in (5), since it can be shown that both formulations yield the same optimal solutions $\mathbf{q}_1^\star$ and $\mathbf{q}_2^\star$. The MAX-VAR formulation seeks to find a direction $\mathbf{g} \in \mathbb{C}^{N/2}$ that is maximally correlated after the linear projections of $\mathbf{Y}_1$ and $\mathbf{Y}_2$ on $\mathbf{q}_1 \in \mathbb{C}^{M_s}$ and $\mathbf{q}_2 \in \mathbb{C}^{M_s}$, respectively.

In a recent work [37], we have shown that given two multi-antenna signal views that include one shared (common) component and multiple individual ("private", not shared) components in each view, CCA can efficiently extract the common component up to scaling ambiguity no matter how strong the individual components are. One can see from the two signal views in (10) that each block (view) is subject to strong interference by the primary user, but, in general, the interference is different in the two blocks – thus there is a unique common subspace, namely (the span of) $\mathbf{s}$ that conveys the secondary transmission. Building upon our theoretical findings in [37], we will next show that our CCA interpretation applies, and under very mild conditions will recover $\mathbf{s}$ up to scaling , even if $\mathbf{x}_p$ is several orders of magnitude stronger than $\mathbf{x}_s$.

The following theorem, which is a slight modification of the results of [30], states the conditions for identifying the secondary transmitted signal $\mathbf{s}$ at the SRx.

**Theorem 1.** *In the noiseless case, if the matrices $\mathbf{B}_\ell := [\mathbf{s}, \mathbf{p}_\ell] \in \mathbb{C}^{N/2\times 2}$, for $\ell \in \{1,2\}$, and $\mathbf{H}_s \in \mathbb{C}^{M_s \times 2}$ are full column rank, then the optimal solution $\mathbf{g}^\star$ of problem* (12) *is given by $\mathbf{g}^\star = \gamma\mathbf{s}$, where $\gamma \in \mathbb{C}$, $\gamma \neq 0$ is the scaling ambiguity.*

*Proof.* The proof is provided in Theorem 1 in [37]. □

Note that the full rank condition on the matrices $\mathbf{B}_\ell$ needs the signals $\mathbf{s}$ and $\mathbf{p}_\ell$ to be linearly independent which is practically always the case for any reasonable "packet" length $N$, because these signals are drawn from statistically independent sources. On the other hand, the full rank condition on $\mathbf{H}_s$ is in fact the more restrictive one as it requires i) the number of antennas at the SRx to be greater than or equal to the number of co-channel signals (two in our setting) and ii) the channel vectors to be linearly independent. The latter is realistic, these being statistically independent channel vectors from the PTx and the STx to the SRx.

To further show how well our approach works in the presence of noise, we provide theoretical analysis of the correlation coefficient between the estimated and the transmitted secondary signal in the presence of noise, as $N \to \infty$. We have the following result.

**Proposition 1.** *In the presence of additive white complex circularly symmetric Gaussian noise of variance $\sigma_s^2$ ($_s$ for secondary Rx noise), as the packet length, $\frac{N}{2}$, goes to infinity, the correlation coefficient between the optimal solution $\mathbf{g}^\star$ of problem* (12) *and the true signal $\mathbf{s}$ approaches*

$$\rho = \sqrt{\frac{|\mathbf{z}_s(1)|^2}{\lambda_1 + \sigma_s^2} + \frac{|\mathbf{z}_s(2)|^2}{\lambda_2 + \sigma_s^2}}, \tag{13}$$

*where*

$$\lambda_{1,2} = \frac{(p_s + p_p) \pm \sqrt{p_s^2 + p_p^2 + 2p_p p_s(1 - 2\cos(\gamma))}}{N},$$

$p_s = \alpha_s \|\mathbf{h}_s\|^2 \frac{N}{2}$, $p_p = \alpha_p \|\mathbf{h}_p\|^2 \frac{N}{2}$, *$\gamma$ is the angle between the vectors*

$$\mathbf{w}_{\sqrt{\alpha_s}\mathbf{h}_s} = [\alpha_s |\mathbf{h}_s(1)|^2, \alpha_s |\mathbf{h}_s(2)|^2, -j \cdot \alpha_s \mathbf{h}_s(1)^* \mathbf{h}_s(2), \\ - j \cdot \alpha_s \mathbf{h}_s(1)\mathbf{h}_s^*(2)]$$

*and*

$$\mathbf{w}_{\sqrt{\alpha_p}\mathbf{h}_{ps}} = [\alpha_p |\mathbf{h}_{ps}(2)|^2, \alpha_p |\mathbf{h}_{ps}(1)|^2, j \cdot \alpha_p \mathbf{h}_{ps}^*(1)\mathbf{h}_{ps}(2), \\ j \cdot \alpha_p \mathbf{h}_{ps}(1)\mathbf{h}_{ps}^*(2)],$$

*while for $i = 1, 2$,*

$$\mathbf{z}_s(i) = \frac{y_i^* \sqrt{\alpha_s}\mathbf{h}_s(1) + \sqrt{\alpha_s}\mathbf{h}_s(2)}{\sqrt{|y_i|^2 + 1}}, \text{ where} \\ y_i = \frac{\lambda_i - \alpha_s |\mathbf{h}_s(2)|^2 - \alpha_p |\mathbf{h}_{ps}(2)|^2}{\alpha_s \mathbf{h}_s(2)\mathbf{h}_s^*(1) + \alpha_p \mathbf{h}_{ps}(2)\mathbf{h}_{ps}^*(1)}. \tag{14}$$

*Proof.* The proof is relegated to Appendix I. □

Note that we only provide a short version of the proof due to the space limitation. The detailed version of the proof, the experimental verification, and an insightful discussion highlighting the impact of SNR and the users' channel correlation are deferred to the supplement.

### *A. Time-varying Channel Directions, Fading, and Intermittent Transmissions.*

Although the two signal views in (10) implicitly assume that the channel is constant across the two secondary repetition blocks, our proposed method in fact works even if the two channel matrices are different [37]. Therefore, with block repetition, the coherence time needs to be only greater than one block duration. We will see in the experiments how this feature grants our proposed method robustness against time varying channels.

### *B. Interference Cancellation?*

It is worth pointing out that if the primary user signal is order(s) of magnitude stronger and the primary channel remains constant (no intermittent transmissions, no time-division duplex, insignificant channel direction changes) then one can cancel the primary interference by simply projecting the received signal on the minor left singular vector of the matrix $\mathbf{Y}_\ell$, thereby "revealing" the secondary transmission. This can only work when the spatial channels are time-invariant. In practice, the channel gains fluctuate over time, and even if the average secondary signal to interference ratio is low (e.g., -40 dB), there are times when it becomes relatively high (e.g., -20 dB). These fluctuations quickly degrade the subspace estimate, leading to complete failure to detect the secondary signal, as we will see in the laboratory experiments.

### C. Multiple Secondary Users

Note that our theoretical results dictate that our proposed CCA approach can identify the secondary signal in a network with only one secondary user, and we have argued that finding the secondary user signal is tantamount to solving for a principal eigenvector which can be cheaply computed via the power method. Even with multiple secondary users, our recovery claim holds and receiver complexity is roughly the same, provided that i) each secondary receiver has enough antennas (as many as the maximum number of active users at any given time, see Theorem 1); and ii) there are no persistent and perfectly aligned collisions between any of the secondary users. In other words, no two secondary users transmit their packet pairs at the exact same times. With asynchronous wake-up type devices serving intermittent communication needs, this situation is highly likely.

## VI. Secondary Synchronization

One critical issue that we always face in practice is synchronization. The overall synchronization task comprises time, carrier frequency offset (CFO), and phase synchronization. While effective solutions to these problems are well-established for classical communication modalities, here we are dealing with a secondary signal that is potentially buried under the primary one, which makes secondary time synchronization and CFO acquisition much more challenging.

A standard receiver will naturally lock on the primary user, which means that the secondary signal will present itself with an unknown CFO and unknown start time within the received sequence. Fortunately, the presence of CFO does not destroy the alignment of the two copies of the secondary packet: owing to the temporal shift invariance property of pure complex exponential signals, the second copy is the same as the first except for a complex phase shift. Hence we can proceed with CCA and correct the CFO after recovering the CFO-modulated secondary packet. On the other hand, secondary timing acquisition is a challenge, due to the large power imbalance between the primary and the secondary signal. To deal with this problem, we propose a blind CCA-based algorithm that is practically effective in finding the start time of the secondary packet under such a large power imbalance between the two users.

In practice, the secondary receiver receives a long sequence, $\widetilde{\mathbf{Y}}_s \in \mathbb{R}^{M_s \times \widetilde{N}}$ where $\widetilde{N} > N$. The goal is to find the sample index, $k$, so that we can extract the desired signal $\mathbf{Y}_s$ from $\widetilde{\mathbf{Y}}_s$, and then use the proposed method in Section V to decode the secondary user signal.

By exploiting the repetition structure of the transmitted signal, we start with $k = 1$ and construct the two views $\mathbf{Y}_1^{(k)} = \widetilde{\mathbf{Y}}_s(:, k : N/2 + k - 1)$ and $\mathbf{Y}_2^{(k)} = \widetilde{\mathbf{Y}}_s(:, N/2 + k : k + N - 1)$ followed by solving (2) to obtain the associated correlation coefficient $\rho_k$.[1] Then, we store $\rho_k$, set $k = k + 1$ and repeat the previous procedure. If we hit the start point of the two copies of the same packet, then CCA of these "views" will yield its maximum correlation coefficient. In other words, the correlation coefficient, $\rho_k$ defined in (3), associated with each pair of canonical directions $\mathbf{q}_1^{(k)}$ and $\mathbf{q}_2^{(k)}$ obtained by solving (5) at the $k$-th step, will be at its maximum only when we have all the $N/2$ symbols in both views. This is because, under the usual assumption that the secondary information sequence is uncorrelated, even if $k$ is off by one, the two partial sequences will decorrelate. The higher $N$ is, the higher the correlation peak we obtain as we will see in the experiments, but even moderate $N$, in the order of 128 symbols, can yield very good detection performance. Notice that the procedure utilizes the special frame structure that is designed to enable CCA, but is otherwise agnostic to the specific information sequence that is being sent by the secondary transmitter. In this sense, it is a blind synchronization strategy that leverages the power of CCA to enable reliable timing acquisition at very low SINR. The procedure is summarized as Algorithm 1.

[1] We use MATLAB notation, i.e., $\mathbf{X}^{(k)} = \mathbf{X}(:, k : N + k - 1)$ contains all the rows of matrix $\mathbf{X}$ and a subset of columns of $\mathbf{X}$ starting from the $k$-th column and ending with the $(N + k - 1)$-th column.

**Algorithm 1** Secondary Synchronization

**Input**: $\widetilde{\mathbf{Y}}_s \in \mathbb{C}^{M_1 \times \widetilde{N}}$,
**Initialization**: $k = 1$,
**while** $k \in [\widetilde{N} - N + 1]$ **do**
  Construct $\mathbf{Y}_1^{(k)} = \widetilde{\mathbf{Y}}_s(:, k : N/2 + k - 1)$ and $\mathbf{Y}_2^{(k)} = \widetilde{\mathbf{Y}}_s(:, N/2 + k : k + N - 1)$
  Compute $\rho_k$ after solving (5) using $\mathbf{Y}_1^{(k)}$ and $\mathbf{Y}_2^{(k)}$
  Store $(k, \rho_k)$ in a stack
  Set $k := k + 1$
**end**
**Selection**: pick the $k^\star := \max_k \rho_k$.

The computational complexity of Algorithm 1 is determined by the complexity of solving a series of CCA problems, which is equivalent to solving for the principal component (canonical pair) of (2) a number of times (equal to the search window size). The canonical pair can be cheaply computed via a power iteration. Further, each CCA problem requires inversion of correlation matrices of size $M_s \times M_s$ each – these inverses can be computed analytically since $M_s = 2$. To minimize the search window length, one can start with a coarse estimate for the region with high correlation coefficient and then do a narrow search within a small window size to get the final start time index, as we will see in the experiments. Furthermore, if the secondary transmitter is continuously transmitting, we do not need to run the full Algorithm 1 for each received packet – we only need to do a narrow timing search to compensate for jitter.

## VII. Numerical Results

In this section, we will evaluate the proposed method using both simulations and real experiments. We first present simulations to test the performance of the proposed method under different number of antennas, modulation schemes, and fading scenarios. Then, we present experiments using real radios to show how the proposed method works under practical considerations such as synchronization and hardware impairments.

To benchmark the performance of the proposed CCA approach, we use the following baselines.

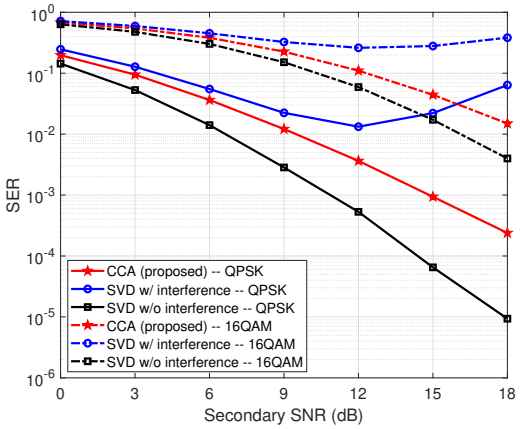


Fig. 2: Secondary user performance under different modulation schemes.

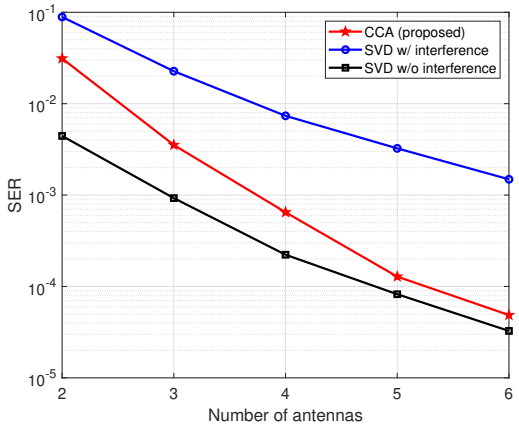


Fig. 3: Secondary user SER versus number of antennas at the SRx.

**SVD without interference:** we will use the singular value decomposition (SVD) to estimate the channel direction during a period when the primary user is inactive, i.e., there is no interference from the primary user. To do that, we first exploit the repetition structure to construct the signal $\mathbf{Y} = [\mathbf{Y}_1^T \mathbf{Y}_2^T]^T \in \mathbb{C}^{2M_s \times N/2}$. Then, the secondary user signal can be estimated by projecting the received signal $\mathbf{Y}$ on the left principal vector. Note that our use of the SVD "baseline" without interference (which is more appropriately called an "oracle" method here) is purely to show how well the proposed method works – close to an oracle which operates in a fictitious interference-free environment.

**SVD with interference:** we will use SVD to project away the interference subspace by projecting on the third principal component of the matrix $\mathbf{Y}$ to estimate the secondary signal. Notice that projecting on the first two components yields the subspace containing the primary user signals, $\mathbf{p}_1$ and $\mathbf{p}_2$.

### *A. Simulations*

We provide simulation results to assess the performance of the proposed CCA approach. We consider the underlay scenario shown in Fig. 1. The transmit power at the PTx, $\alpha_p$, is set to 20 dBm while the maximum transmit power at the STx, $\alpha_s$, is set to 10 dBm. The large scale fading parameters (path-loss) used in the simulation are set to $\sigma_{ss}^2 = -80$ dB, $\sigma_{sp}^2 = \sigma_{ps}^2 = -80$ dB, and the additive white Gaussian noise power is set to $\sigma_s^2 = -88$ dBm. The small scale fading parameters are modeled as circularly symmetric Gaussian random variables with zero mean and variance $1/\sqrt{M_s}$. Furthermore, the total number of samples collected at the SRx is assumed to be 1024, so the repetition is done over two blocks, each of length 512 samples. We conducted $10^4$ Monte-Carlo two-block-transmission experiments, each time drawing new $\mathbf{s}, \mathbf{p}, \mathbf{W}$ and $\mathbf{H}_s$. We assume that the PTx is sending a 32-QAM signal, while the STx is sending a QPSK signal unless stated otherwise. Since we assume digitally-modulated symbols at the secondary user, we will use the symbol error rate (SER) as a performance metric (but recall that our method can also work with analog transmissions).

In the first experiment, we tested the proposed method under different modulation schemes. We varied the STx power from $-8$ dBm to 10 dBm which corresponds to the received SNR range in Fig. 2. For each value of the secondary SNR, we report the corresponding SER obtained by our proposed CCA method and the considered baselines. Fig. 2 shows the SER performance of the proposed method under QPSK and 16-QAM constellations. It is clear that the proposed method approaches the performance of the interference-free SVD baseline even for the higher order modulation case. Further, one can see that the performance of the SVD with interference breaks when the SNR increases (12 dB corresponding to 16 dB power difference between the two users) due to subspace leakage that significantly deteriorates the detection performance. We will show later through real experiments that the gap between the proposed method and SVD with interference is even much larger due to the power fluctuations as will be explained later.

Next, we simulated another experiment to see the impact of the number of antennas at the SRx. We varied the number of antennas ($M_s$) from 2 to 6 while the secondary SNR is fixed at 11 dB (corresponding to 17 dB power difference between the two transmitters). One can see from Fig. 3 that increasing the number of antennas at the SRx brings the proposed method closer to the interference-free SVD. Note that there is no antenna gain here as the channel vectors are normalized with the number of antennas. The reason that the two curves (red and black) in Fig. 3 attain the same performance when $M_s$ exceeds 5 is that the two channels $\mathbf{h}_s$ and $\mathbf{h}_{ps}$ tend to be more uncorrelated when we increase the number of antennas.

Finally, to show how changing the secondary channels across the two blocks affects the performance of the proposed method, we simulated another experiment with completely different channel vectors across the two blocks for both primary and secondary users. For each Monte-Carlo trial, each of the two channels for each user is randomly drawn from a complex Gaussian distribution. Fig. 4 shows that using different channels in the two blocks yields a roughly 3 dB SNR gain. This is attributed to the fact that two different

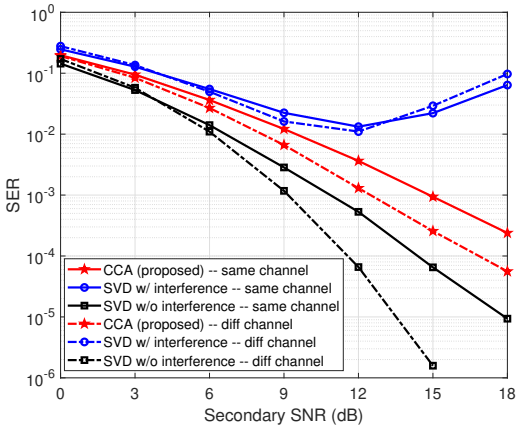


Fig. 4: Secondary user performance with different channel across two blocks, with QPSK modulation.

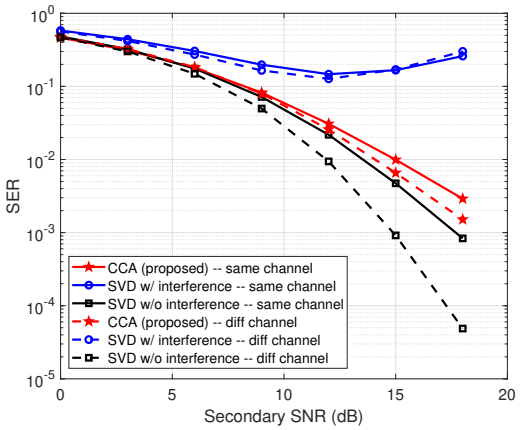


Fig. 5: Secondary user performance with different channel across two blocks, with 8PSK modulation.


Fig. 6: Experimental Setup.

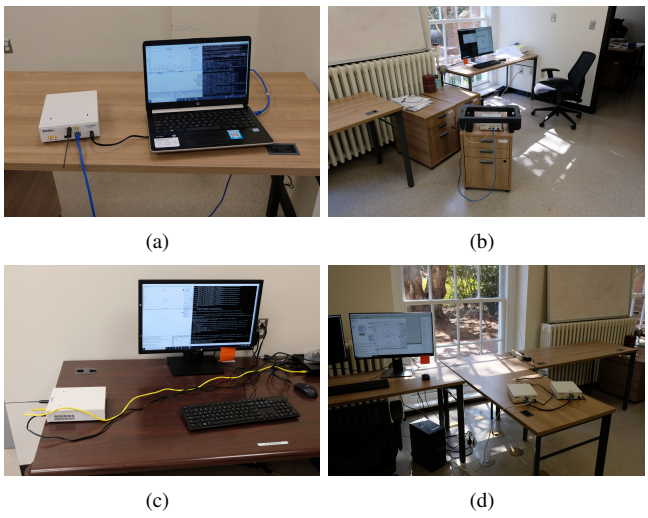

(a) (b) (c) (d)

Fig. 7: (a) Primary Transmitter. (b) Primary Receiver. (c) Secondary Transmitter. (d) Secondary Receiver.

channels will result in a diversity gain. Such a gain increases the probability of seeing more uncorrelated channels ($h_s$ and $h_{ps}$) in any of the views, and this naturally yields a better CCA solution as compared to the case with constant channels across the two blocks.

### *B. Experiments*

In this section, we evaluate the performance of the proposed CCA approach for low-power secondary underlay communication in practice (for simplified simulations, see [1]). To do so, we have built a prototype of the proposed CCA underlay scheme using software defined radios (SDR).

### *C. Experimental Setup*

Both the primary and secondary links are realized using USRP-2920 devices and general-purpose computers. The USRPs are used for radio signal transmission / reception, while the computers are used for baseband signal processing. The experimental layout is shown in Fig. 6. We used five USRPs: one for the primary transmitter, one for the primary receiver, one for the secondary transmitter, and two for the secondary receivers, see Fig. 6. Each USRP is equipped with a single antenna. The two USRPs of the secondary receiver are connected together with a MIMO cable to synchronize the two receive radio frequency chains, as shown in Fig. 7(d).

The locations of the PTx, PRx, STx, SRx are fixed throughout the experiments. The distances between the PTx and PRx, PTx and SRx, STx and PRx, and STx and SRx are 5, 3, 4.5, and 4 meters, respectively. The transmit power of the PTx is set to the maximum possible value, as shown in Table I unless stated otherwise, while the transmit power of the STx is adjusted for low-power secondary transmission. The sampling rate for both users is set to 1 Mega samples per second (MS/sec), the signal bandwidth is 100 KHz, and the carrier frequency is 1.2 GHz. The PTx uses a block of 256 QPSK symbols and the STx uses repetition over two blocks, each of length 128 QPSK symbols. The parameter settings for our experiments are summarized in Table I.

**Signal processing at the transmitters.** At each Tx, the constructed block is oversampled by a factor of 10, then the resulting oversampled signal is pulse-shaped using a square-root raised cosine (SRRC) with roll-off factor and amplitude set to 0.5 and 6, respectively. The pulse shaped signal is

| Parameter | Primary | Secondary |
|---|---|---|
| Bandwidth (KHz) | 100 | 100 |
| Carrier frequency (GHz) | 1.2 | 1.2 |
| Modulation | QPSK | QPSK |
| Sample rate (MSps) | 1 | 1 |
| Maximum transmit power (dBm) | 20 | -15 |
| Number of antennas | 1 Tx, 1 Rx | 1 Tx, 2 Rx |
| Number of symbols | 256 | 128 |
| Oversampling factor | 10 | 10 |
| Number of packets | 2000 | 2000 |

TABLE I: Parameter settings for the experiments.

zero-padded with a number of zeros equal to one third of the packet, yielding a sequence of length $4020$ samples. This results in a transmission rate of 128 Kbps for the primary user and 64 Kbps for the secondary user. The zero-padding (used to emulate intermittent packet transmission) is also used at the receiver side to measure the received SNR and SINR, as we will see later. Symbol generation, up-sampling, and pulse shaping are done in MATLAB. Then, the transmit data of each user is fed to GNU radio before being transmitted over the air.

**Secondary receiver.** We use the proposed CCA algorithm in Section VI to detect both the secondary packet and the start of the $256 \times 2$ complex signal. After SRRC matched filtering, down-sampling to the symbol rate, and secondary synchronization, we construct the two signal views by separating the two back-to-back blocks, and then use CCA to recover the secondary signal. After solving the CCA problem (5), we average the two soft estimates of $\mathbf{s}$ obtained via $\mathbf{Y}_1^H \mathbf{q}_1$ and $\mathbf{Y}_2^H \mathbf{q}_2$, before hard thresholding.

In order to resolve the scaling ambiguity that is inherent both in the proposed CCA method and the SVD-based baselines, we assume that the first four secondary symbols are known at the SRx. Note that these symbols can be drawn from the packet header that contains the STx identification sequence.

**Remark 1.** *It is worth noting that for the second baseline (SVD with interference), we use our proposed* blind *method in Section VI to recover the secondary packet start time index at the SRx, thereby giving a big advantage to the SVD based method. The typical synchronization method that would be used with SVD is to allow the STx to transmit a long pilot sequence, long enough to make up for the large power difference between the two users. Then, we would use knowledge of this pilot sequence at the SRx to find the start time index of the secondary signal via cross-correlation / matched filtering. This would seriously reduce the transmission rate of the secondary user relative to our proposed blind method, especially for the setting considered herein where the secondary user is much weaker than the primary. Further, and perhaps worse, such training-based timing recovery requires the SRx to estimate the secondary CFO before (or together with) timing synchronization, which is in another serious complication given the low SINR and moderate SNR of the secondary user.*

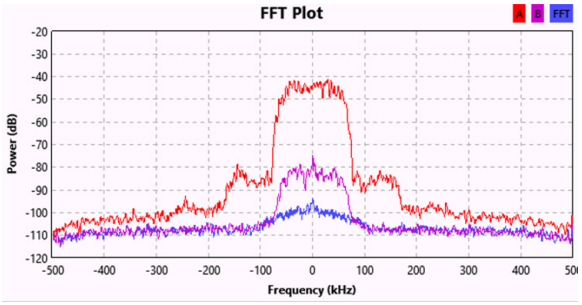


Fig. 8: GNU radio spectrum analyzer showing 40 dB received power difference between the PTx and STx at the SRx. The received signal of the PTx is shown in red while that of the STx is depicted in purple, and the noise in blue.

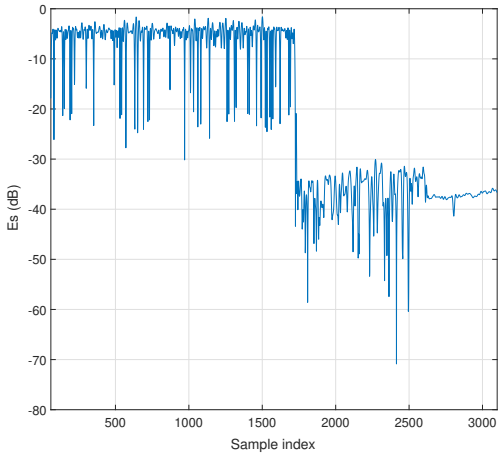


Fig. 9: Squared samples of one of the received packets after matched filtering with the SRRC. Notice the overlap between part of the secondary packet and the zeros of the primary, and also the low SNR of the secondary.

**Primary receiver.** At the PRx, we use energy detection for the primary packet detection. Then, we use primary training symbols to detect the start index of the $256 \times 1$ received signal of the primary user. To decode the primary symbols, we use 10 training pilots to estimate the primary channel coefficient and then do the hard detection of the equalized signal.

### *D. Performance Evaluation*

Since we assume digitally-modulated signals for both users, we will use the symbol error rate (SER) as a performance metric (but recall that our method can also work with analog modulation for the primary and the secondary user).

In the first experiment, we test the performance of the proposed approach under different levels of primary interference at the secondary receiver. To do so, we fix the secondary transmit power to $-18$ dBm. This makes the corresponding measured average received SNR at the SRx equal to approximately $8$ dB. We vary the primary transmit power from $0$ to $20$

dBm in 5 dB steps, thus generating transmit power differences from approximately $-20$ dB down to a rather extreme $-40$ dB. To validate the power difference between the two users at the SRx, Fig. 8 shows the GNU radio spectrum analyzer at the SRx with the received signal strength level of the PTx and STx in addition to the noise level. The transmit power of the PTx is set to 20 dBm, and Fig. 8 shows close to 40 dB power difference between the two users. Furthermore, Fig. 9 depicts the squared samples of one of the received packets at the SRx after matched filtering with the SRRC, for primary transmit power set to 15 dBm. It is clear that part of the secondary transmitted packet overlaps with the padded zeros of the primary packet, showcasing the power difference between the two users. Further, the remaining zeros show the low received SNR range of the secondary user.

| Tx power difference (dB) | 20 | 25 | 30 | 35 | 40 |
|---|---|---|---|---|---|
| SINR ($1^{st}$ antenna ) | -17.1213 | -20.1632 | -27.1965 | -29.1996 | -32.2388 |
| SINR ($2^{nd}$ antenna) | -15.1248 | -18.1909 | -25.2433 | -30.2522 | -31.2015 |

TABLE II: Estimated secondary SINR at the SRx over the two receive channels, across the different transmit power imbalance scenarios. The measured average secondary SNR is around 8 dB.

To compute the received SNR and SINR of the secondary signal at the SRx, we exploit the padded zeros in both the primary and secondary signals to measure the noise power, the secondary signal power, and the primary signal power at the SRx. In particular, we estimate the probability distribution of the symbol energy across 1500 packets, each of length 400 symbols. From the distribution, one can estimate either two peaks or three peaks, depending on the overlap between the secondary (primary) and the zeros of the primary (secondary). For instance, Fig. 10(a) clearly shows one of the received packets in one of the channels for the 20 dB transmit power imbalance case. One can clearly see the three different energy levels: one for the (primary, secondary and noise), another for (secondary and noise), and one for noise only. Notice that the first level can also be primary and noise, but since the primary is very strong, treating the first level as (primary and noise) or (primary, secondary and noise) will have negligible impact on the SINR and SNR measurements of the secondary user. Fig. 10(c), shows the histogram of the collected data across 1500 packets for the 20 dB transmit power difference, where three distinct peaks are observed. In Fig. 10(b), however, one can see a complete overlap between part of the secondary signal and the padded zeros of the primary user for the 40 dB transmit power difference, and hence, only two peaks can be seen in the distribution shown in Fig. 10(d).

We use the data collected for the 20 dB transmit power difference to measure the energy levels corresponding to the three observed probability density peaks, see Fig. 10(c). We use these values to solve a system of linear equations (three equations in three unknowns) to compute the received SNR and SINR at the secondary receiver. We repeat the same procedure for the different transmit power difference cases to calculate the associated SINR and SNR values. Note that,

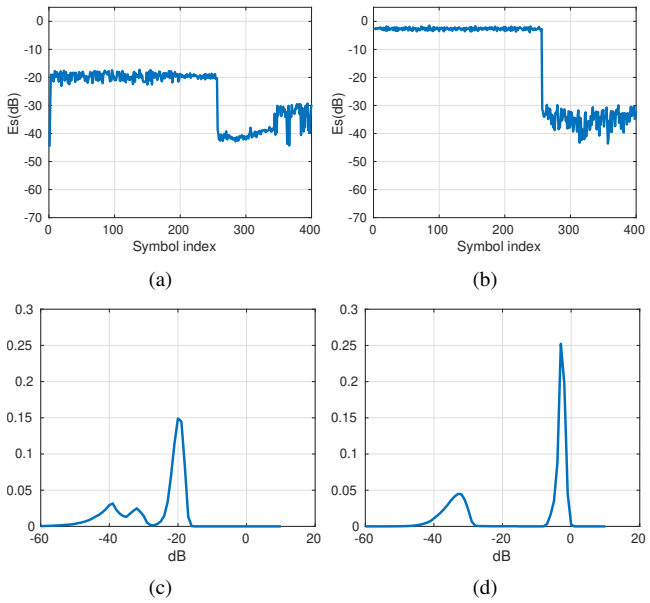


Fig. 10: Example of the received primary user's packets at the SRx after matched filtering with the SRRC for 20 dB and 40 dB transmit power difference. Plots a) and b) depict the symbol energy of the detected packet, for the two transmit power imbalance scenarios, while (c) and (d) correspond to the estimated probability distribution of the energy (in dB) of the detected symbols for the 20 dB and 40 dB transmit power difference cases, respectively.

since the secondary transmit power is fixed throughout this experiment, we observed approximately the same average energy level (peak value) for either the noise level or the (secondary and noise) level, across all the transmit power difference cases. However, as expected, we observed increase in the estimated energy level that corresponds to the primary, secondary and noise. To confirm this, one can see from Fig. 10(b) a complete overlap between part of the secondary signal and the padded zeros of the primary user for the 40 dB transmit power difference case, and hence, only two peaks can be seen in the distribution shown in Fig. 10(d). Notice that the energy level associated with the smallest peak (secondary and noise) in Fig. 10(d) is roughly equivalent to the energy level associated with the middle peak in Fig. 10(c), while one can easily see close to 20 dB increase in the highest peak (primary, secondary and noise) in Fig. 10(d) relative to Fig. 10(c). The measured SINR values for the different transmit power cases are reported in Table II.

In order to demonstrate the capability of our proposed approach to correctly decode the secondary transmission at very low SINR, we report the SER of the secondary user obtained by our proposed CCA method at five different levels of the (average) transmit power imbalance: from $-20$ dB to $-40$ dB (corresponding secondary SINR levels are reported in Table II). Fig. 11 depicts SER results obtained by our proposed CCA method, for all five levels of primary interference, and the corresponding SER curve obtained using the SVD-based method at the same SNR *without any interfer-*

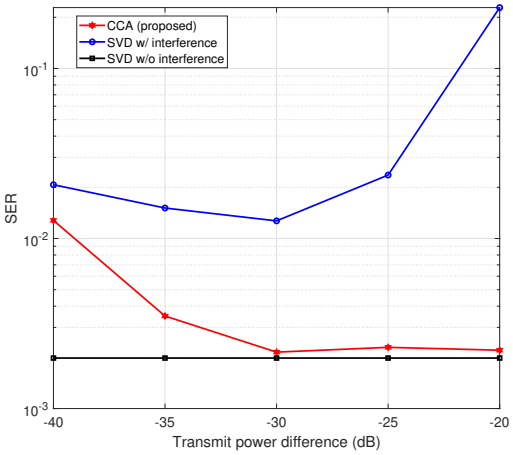


Fig. 11: Secondary user detection performance at different average SINR levels. The measured average secondary SNR is approximately 8 dB.

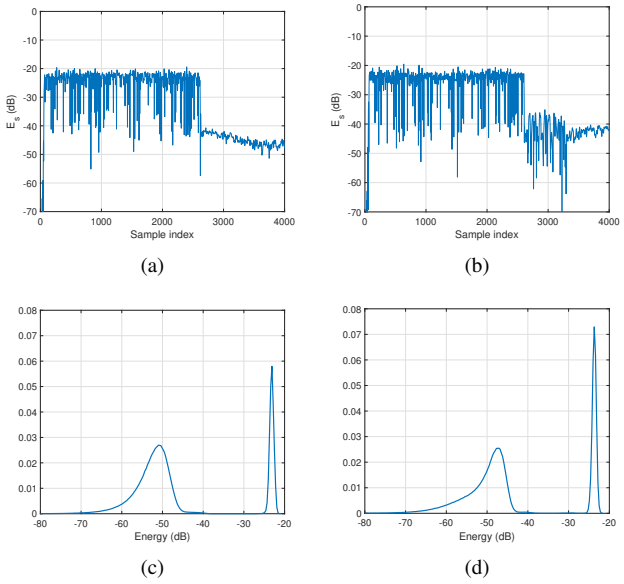


Fig. 12: (a) primary packet samples when the STx is inactive. (b) primary packet samples when the STx is active. (c) energy distribution when the STx is inactive. (d) energy distribution when the STx is active.

*ence*. The results are striking: CCA is remarkably insensitive to interference from the primary user. In particular, CCA achieves almost the same performance at power difference levels $(-35, -30, -20, -25)$ dB. On the other hand, at the $-40$ dB level, the CCA performance degrades. This mainly happens due to the limited resolution of the analog to digital converter of our USRP for the wide dynamic range of the input signal – while the average SINR is $-32$ dB, there are several instances where it drops below $-40$ dB, and these occasional quantization errors ultimately dominate CCA performance. Despite that, CCA still achieves close to $10^{-2}$ SER. Finally, one can see that CCA significantly outperforms the SVD method used for interference cancellation, even though the latter is in fact aided by the CCA frame structure to acquire timing – a benefit which it won't have in practice. As shown in Fig. 11, SVD performance breaks at 25 dB transmit power difference, where primary subspace estimation becomes very difficult, and hence interference cancellation does not work.

Considering the primary user's performance, we observed that the single-antenna primary receiver is completely insensitive to the secondary interference. Fig. 12(a) shows one of the received packets at the PRx (before down sampling), with the primary transmit power set to 0 dBm (minimum primary power in this experiment), while the secondary user is inactive. On the other hand, Fig. 12(b) shows one of the received packets at the PRx (before down sampling) when the secondary user is active, where there is approximately $70\%$ overlap between the two users' packets. We observed that in the worst case setting, where the primary user power is fixed to its minimum level (highest interference from the secondary user), the same detection performance can be attained regardless whether the secondary user is active or not. This is due to the fact that the secondary interference is close to the primary's noise floor, as one can see from Fig. 12(c) and Fig. 12(d), where the two smaller peaks in Fig. 12(c) and Fig. 12(d) correspond to the noise level and the secondary plus noise level, respectively. We observed that the SNR of the primary user is 28 dB when the secondary user is inactive, while the primary user's SINR is 25 dB when the secondary user is active.

**Effect of secondary SNR.** We consider another experiment to see the performance of the proposed method under different SNR values for the secondary user. To do so, we fixed the primary transmit power to 10 dBm and varied the secondary transmit power from $-23$ to $-17$ dBm which corresponds to average SNR values between 2 dB and 10 dB, as observed. At each SNR value, we report the SER of the secondary user. Fig. 13 depicts the SER performance of the secondary user versus its SNR. It is obvious how well our proposed method works at very low SNR / SINR values. In particular, our method can achieve $10^{-2}$ SER at 7 dB and closely approaches what is attained by the interference-free SVD baseline at low SNR values. Further, one can see that the SVD with interference completely fails at both the low SNR and high SNR regions, where in the latter, the secondary user becomes a bit more stronger and then accurate primary subspace estimation becomes more difficult as explained in the previous experiment.

On the other hand, we observed that the secondary user does not affect the primary performance, which remains the same as is attained when the secondary user is inactive. The same SER is observed at the PRx, even at the extreme case where the secondary transmit power is $-17$ dBm (i.e., the highest interference to the primary).

**Impact of packet size.** We test the performance of the proposed method as a function of secondary packet size. The secondary and primary transmit powers are fixed to $-20$ dBm and 5 dBm, respectively. The measured average

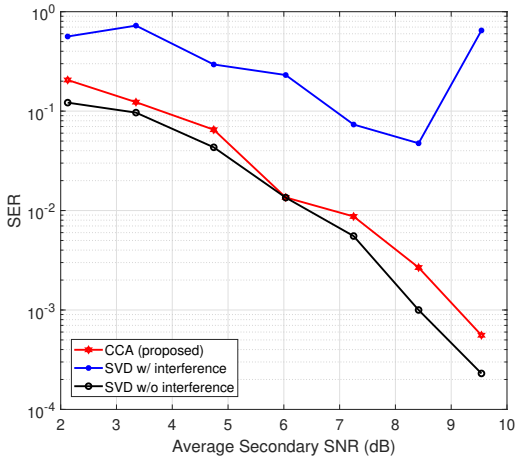


Fig. 13: Secondary user detection performance at different SNR.

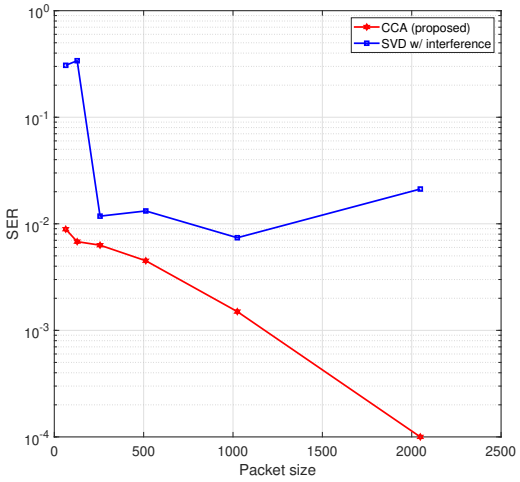


Fig. 14: Secondary user detection performance for different packet sizes of the secondary user. The packet length of the primary user is fixed to 256 QPSK symbols.

SNR at the secondary receiver is 7 dB. The primary packet length is set to 256 QPSK symbols. Fig. 14 shows the SER performance of the proposed approach versus the packet size of the secondary user. We observe a significant improvement in the secondary SER when the secondary packet length increases. This is due to the fact that increasing $N$ renders the transmit sequences closer to being orthogonal and having low auto-correlation sidelobes, which improves the performance of CCA and secondary timing synchronization. We recently established a performance analysis of CCA in [37], where we showed that increasing the packet length yields higher canonical correlation coefficient, and hence a better estimate for the common signal. This suggests that transmitting longer secondary packets provides better secondary detection performance. On the other hand, one can argue that if the channel is fast time varying, then the higher the packet length, the higher the probability of each block being subject to channel

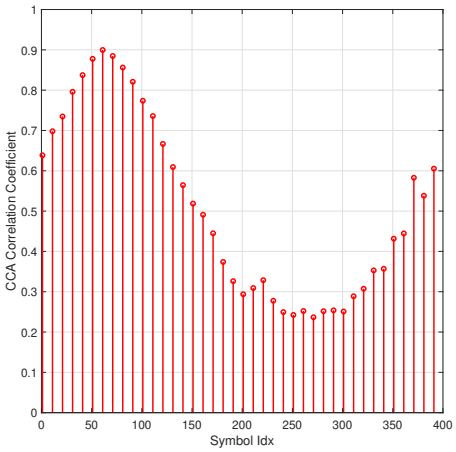


Fig. 15: Secondary user synchronization using CCA.

variation, thus violating the presumed mode. Hence, in setting the secondary packet length one has to take into account the coherence time of the channel, in order to choose the optimal packet length for the secondary user.

**Secondary synchronization.** Finally, we evaluate the performance of the proposed algorithm for finding the start time of the secondary packet. We use the same parameters as the previous experiment but the secondary packet is fixed to 256 symbols. Recall that the received packet length, before downsampling, is 4020 samples. To find the start of the $256 \times 2$ signal, we run Algorithm 1 with a step of 10 symbols on the received signal, which resulted in solving approximately a series of 40 CCA problems. Fig. 15 shows that the highest correlation coefficient is attained at symbols index 60. We then performed an additional narrow (fine) search over a window size of 10 symbols centered at the obtained symbol index from the wide search.

## VIII. Conclusions

In this paper, we proposed a practical low-complexity data-driven spectrum sharing approach for an asynchronous underlay scenario involving a high-power primary user and a low-power secondary link. The proposed method allows the secondary user to reliably communicate over the same channel occupied by the primary, without any coordination, and without any channel state information. Our proposed solution is based on "repetition coding": the secondary user transmits its signal twice at very low power such that it does not affect the primary user detection performance. Constructing two signal views at the SRx and applying CCA to these views, we showed that the secondary receiver can reliably decode its intended signal at moderate SNR even if it is buried under strong interference from the primary user transmission. We proposed a low-complexity unsupervised based approach that can resolve the crucial low-SINR synchronization issue at the secondary receiver. Laboratory experiments using a custom-built USRP testbed confirmed the efficacy of the proposed method in decoding the secondary signal at very low SINR in real world wireless environments.

The proposed framework can guarantee reliable reception of the secondary underlay signal even under time-varying and intermittent interference from the primary user. Specifically, our theoretical results show that the secondary signal can be identified even if the primary channel is different across the two secondary signal blocks. To the best of our knowledge, this is the first spectrum underlay work that allows a low-power secondary user to occupy the channel with a time varying primary user in a realistic wireless environment, without i) requiring any knowledge about the primary network (waveform, modulation, channel, timing, etc.), ii) coordination between the primary and the secondary system, iii) long pilot sequences for acquisition and channel estimation for the secondary user.

## APPENDIX
## PROOF OF PROPOSITION 1

Let us write the model for the two constructed views in equations (10) and (11) in more compact form as

$$\mathbf{Y}_\ell = \left[\sqrt{\alpha_s}\mathbf{h}_s \quad \sqrt{\alpha_p}\mathbf{h}_{ps}\right]\left[\mathbf{s} \quad \mathbf{p}_\ell\right]^T + \mathbf{W}_\ell, \tag{15}$$

for $\ell = 1, 2$, where each element of $\mathbf{W}_\ell$ has zero mean and variance $\sigma_s^2$, for all $\ell = 1, 2$. The solution of problem (12) is given by the solution of the following generalized eigenvalue problem

$$\mathbf{R}_{12}\mathbf{R}_{22}^{-1}\mathbf{R}_{21}\mathbf{q}_1 = \lambda\mathbf{R}_{11}\mathbf{q}_1, \tag{16}$$

where $\mathbf{R}_{ij} = \frac{2}{N}\mathbf{Y}_i\mathbf{Y}_j^H$. Given the model in (15) and since $\|\mathbf{s}\|^2 = \|\mathbf{p}_1\|^2 = \|\mathbf{p}_2\|^2 = N/2$, one can see that

$$\mathbf{R}_{ij} \approxeq \alpha_s\mathbf{h}_s\mathbf{h}_s^H + \delta_{i,j}\left(\alpha_p\mathbf{h}_{ps}\mathbf{h}_{ps}^H + \sigma_s^2\mathbf{I}\right), \tag{17}$$

where $\delta_{i,j}$ denotes the Kronecker delta. Based on relation (17), it can be shown that equation (16) can be rewritten as

$$\alpha_s^2\mathbf{h}_s\mathbf{h}_s^H\hat{\mathbf{A}}^{-1}\mathbf{h}_s\mathbf{h}_s^H\mathbf{q}_1 = \lambda\hat{\mathbf{A}}\mathbf{q}_1, \tag{18}$$

for $\hat{\mathbf{A}} = \mathbf{A} + \sigma_s^2\mathbf{I}$ and $\mathbf{A} = \alpha_s\mathbf{h}_s\mathbf{h}_s^H + \alpha_p\mathbf{h}_{ps}\mathbf{h}_{ps}^H$.

Consider now the eigenvalue decomposition of $\mathbf{A} = \mathbf{U}\mathbf{\Lambda}\mathbf{U}^H$. The eigenvalue decomposition of $\hat{\mathbf{A}}$ is given by $\hat{\mathbf{A}} = \mathbf{U}\left(\mathbf{\Lambda} + \sigma_s^2\mathbf{I}\right)\mathbf{U}^H$. After letting $\mathbf{q}_1 = \mathbf{U}\mathbf{w}_1 = \mathbf{U}\left(\mathbf{\Lambda} + \sigma_s^2\mathbf{I}\right)^{-\frac{1}{2}}\mathbf{b}_1$ and $\sqrt{\alpha_s}\mathbf{h}_s = \mathbf{U}\mathbf{z}_s = \mathbf{U}\left(\mathbf{\Lambda} + \sigma_s^2\mathbf{I}\right)^{\frac{1}{2}}\mathbf{y}_s$, equation (18) becomes

$$\mathbf{y}_s\mathbf{y}_s^H\mathbf{b}_1 = \frac{\lambda}{v_s}\mathbf{b}_1, \tag{19}$$

for $v_s := \frac{\left|\sqrt{\alpha_s}\mathbf{h}_s^H\mathbf{U}(:,1)\right|^2}{\lambda_1+\sigma_s^2} + \frac{\left|\sqrt{\alpha_s}\mathbf{h}_s^H\mathbf{U}(:,2)\right|^2}{\lambda_2+\sigma_s^2} > 0$. Equation (19) is satisfied only when $\mathbf{b}_1 = \alpha_1\mathbf{y}_s$, for $\alpha_1 \in \mathbb{C}$. Substituting $\mathbf{b}_1$ back to equation (19) gives that $\|\mathbf{y}_s\|^2 = \frac{\lambda}{v_s}$, while the expression for $\mathbf{q}_1$ now becomes $\mathbf{q}_1 = \alpha_1\mathbf{U}\left(\mathbf{\Lambda} + \sigma_s^2\mathbf{I}\right)^{-\frac{1}{2}}\mathbf{y}_s$. Since $\mathbf{R}_{11} = \mathbf{R}_{22}$ and $\mathbf{R}_{21} = \mathbf{R}_{12}$ we can easily conclude that $\mathbf{q}_1 = \mathbf{q}_2$. As a result, we can get that the solution of MAX-VAR, in terms of $\mathbf{g}$, is given by $\mathbf{g} = \mathbf{Y}_1^T\mathbf{q}_1^* = \mathbf{Y}_2^T\mathbf{q}_2^*$, with $\mathbf{g}$ satisfying $\|\mathbf{g}\| = \sqrt{N/2}$.

Now, let us consider the cosine of the angle between $\mathbf{g}$ and $\mathbf{s}$, $\phi$. Then, it can be shown that

$$\cos(\phi) := \frac{\left|\mathrm{Re}\left(\mathbf{g}^T\mathbf{s}^*\right)\right|}{\|\mathbf{g}\|\,\|\mathbf{s}^*\|} = \left|\mathrm{Re}\left(\alpha_1\right)\right|\|\mathbf{y}_s\|^2. \tag{20}$$

The term $\alpha_1$ expresses the inherent phase difference that appears between vectors $\mathbf{q}_1$ and $\mathbf{h}_s$. This phase difference can be estimated when pilot symbols are available over the transmission. In that case, the optimal case where the $\cos(\phi)$ is maximized is when $|\mathrm{Re}(\alpha_1)| = |\alpha_1|$. From the constraints $\mathbf{q}_1^H\mathbf{R}_{11}\mathbf{q}_1 = 1$, we can obtain that $|\alpha_1| = \frac{1}{\|\mathbf{y}_s\|}$. As a result, we have that

$$\cos(\phi) = \|\mathbf{y}_s\| = \sqrt{\frac{|\mathbf{z}_s(1)|^2}{\lambda_1+\sigma_s^2} + \frac{|\mathbf{z}_s(2)|^2}{\lambda_2+\sigma_s^2}}. \tag{21}$$

In order to proceed, we will have to specify the eigenvalue decomposition of matrix $\mathbf{A}$. The element-wise representation of matrix $\mathbf{A}$ is given by

$$\mathbf{A} = \begin{bmatrix} \alpha_s|\mathbf{h}_s(1)|^2 + \alpha_p|\mathbf{h}_{ps}(1)|^2 & q^* \\ q & \alpha_s|\mathbf{h}_s(2)|^2 + \alpha_p|\mathbf{h}_{ps}(2)|^2 \end{bmatrix},$$

with $q = \alpha_s\mathbf{h}_s(2)\mathbf{h}_s^*(1) + \alpha_p\mathbf{h}_{ps}(2)\mathbf{h}_{ps}^*(1)$. After using the results presented in [44], we can obtain the eigenvectors and the eigenvalues of matrix $\mathbf{A}$ which are given by $\lambda_1 = \frac{\alpha_s\|\mathbf{h}_s\|^2+\alpha_p\|\mathbf{h}_{ps}\|^2+\delta}{2}$ and $\lambda_2 = \frac{\alpha_s\|\mathbf{h}_s\|^2+\alpha_p\|\mathbf{h}_{ps}\|^2-\delta}{2}$, after letting

$$\delta = \sqrt{\alpha_s^2\|\mathbf{h}_s\|^4 + 2\alpha_s\alpha_p\|\mathbf{h}_s\|^2\|\mathbf{h}_{ps}\|^2(1-2\cos(\gamma)) + \alpha_p^2\|\mathbf{h}_{ps}\|^4}$$

and $\gamma$ be the angle between the vectors

$$\begin{aligned}\mathbf{w}_{\sqrt{\alpha_s}\mathbf{h}_s} = [&\alpha_s|\mathbf{h}_s(1)|^2, \alpha_s|\mathbf{h}_s(2)|^2, -j\cdot\alpha_s\mathbf{h}_s(1)^*\mathbf{h}_s(2),\\ &-j\cdot\alpha_s\mathbf{h}_s(1)\mathbf{h}_s^*(2)]\end{aligned}$$

and

$$\begin{aligned}\mathbf{w}_{\sqrt{\alpha_p}\mathbf{h}_{ps}} = [&\alpha_p|\mathbf{h}_{ps}(2)|^2, \alpha_p|\mathbf{h}_{ps}(1)|^2, j\cdot\alpha_p\mathbf{h}_{ps}^*(1)\mathbf{h}_{ps}(2),\\ &j\cdot\alpha_p\mathbf{h}_{ps}(1)\mathbf{h}_{ps}^*(2)].\end{aligned}$$

Moreover, after letting $p_s = \alpha_s\|\mathbf{h}_s\|^2\frac{N}{2}$ and $p_p = \alpha_p\|\mathbf{h}_{ps}\|^2\frac{N}{2}$, we can get that

$$\lambda_{1,2} = \frac{(p_s+p_p) \pm \sqrt{p_s^2+p_p^2+2p_pp_s(1-2\cos(\gamma))}}{N}.$$

Regarding the eigenvectors of matrix $\mathbf{A}$, let $y_i = \frac{\lambda_i-\alpha_s|\mathbf{h}_s(2)|^2-\alpha_p|\mathbf{h}_{ps}(2)|^2}{\alpha_s\mathbf{h}_s(2)\mathbf{h}_s^*(1)+\alpha_p\mathbf{h}_{ps}(2)\mathbf{h}_{ps}^*(1)}$. Then, we can get that

$$\mathbf{U} = \begin{bmatrix} \frac{y_1}{\sqrt{|y_1|^2+1}} & \frac{y_2}{\sqrt{|y_2|^2+1}} \\ \frac{1}{\sqrt{|y_1|^2+1}} & \frac{1}{\sqrt{|y_2|^2+1}} \end{bmatrix}, \tag{22}$$

while for $\mathbf{z}_s$, we can get that $\mathbf{z}_s(i) = \mathbf{U}(:,i)^H\sqrt{\alpha_s}\mathbf{h}_s = \frac{y_i^*\sqrt{\alpha_s}\mathbf{h}_s(1)+\sqrt{\alpha_s}\mathbf{h}_s(2)}{\sqrt{|y_i|^2+1}}$.

## REFERENCES


[1] M. S. Ibrahim and N. D. Sidiropoulos, "Blind carbon copy on dirty paper: seamless spectrum underlay via canonical correlation analysis," in *IEEE International Conference on Acoustics, Speech and Signal Processing (ICASSP)*, Toronto, Canada, June 2021.

[2] A. Goldsmith, S. A. Jafar, I. Maric, and S. Srinivasa, "Breaking spectrum gridlock with cognitive radios: An information theoretic perspective," *Proceedings of the IEEE*, vol. 97, no. 5, pp. 894–914, Apr. 2009.

[3] S. Haykin, "Cognitive radio: brain-empowered wireless communications," *IEEE Journal on Selected Areas in Communications*, vol. 23, no. 2, pp. 201–220, Feb. 2005.

[4] A. Ghasemi and E. S. Sousa, "Spectrum sensing in cognitive radio networks: requirements, challenges and design trade-offs," *IEEE Communications Magazine*, vol. 46, no. 4, pp. 32–39, Apr. 2008.

[5] T. S. Rappaport, Y. Xing, G. R. MacCartney, A. F. Molisch, E. Mellios, and J. Zhang, "Overview of millimeter wave communications for fifth-generation (5G) wireless networks—with a focus on propagation models," *IEEE Transactions on Antennas and Propagation*, vol. 65, no. 12, pp. 6213–6230, Aug. 2017.

[6] Q. Zhao and B. M. Sadler, "A survey of dynamic spectrum access," *IEEE Signal Processing Magazine*, vol. 24, no. 3, pp. 79–89, May 2007.

[7] J. M. Peha, "Approaches to spectrum sharing," *IEEE Communications Magazine*, vol. 43, no. 2, pp. 10–12, Feb. 2005.

[8] S. Geirhofer, L. Tong, and B. M. Sadler, "Cognitive radios for dynamic spectrum access-dynamic spectrum access in the time domain: Modeling and exploiting white space," *IEEE Communications Magazine*, vol. 45, no. 5, pp. 66–72, May 2007.

[9] Y. Zeng, Y.-C. Liang, A. T. Hoang, and R. Zhang, "A review on spectrum sensing for cognitive radio: Challenges and solutions," vol. 2010, Jan. 2010.

[10] T. Yucek and H. Arslan, "A survey of spectrum sensing algorithms for cognitive radio applications," *IEEE Communications Surveys Tutorials*, vol. 11, no. 1, pp. 116–130, Mar. 2009.

[11] L. M. Lopez-Ramos, Y. Teganya, B. Beferull-Lozano, and S. J. Kim, "Channel gain cartography via mixture of experts," in *IEEE Global Communications Conference (GLOBECOM)*, Taipei, Taiwan, Dec. 2020, pp. 1–7.

[12] A. G. Marques, L. M. Lopez-Ramos, G. B. Giannakis, and J. Ramos, "Resource allocation for interweave and underlay CRs under probability-of-interference constraints," *IEEE Journal on Selected Areas in Communications*, vol. 30, no. 10, pp. 1922–1933, Nov. 2012.

[13] N. Yi, Y. Ma, and R. Tafazolli, "Underlay cognitive radio with full or partial channel quality information." *International Journal of Navigation and Observation*, vol. 2010, July 2010.

[14] D. Denkovski, V. Rakovic, V. Atanasovski, L. Gavrilovska, and P. Mähönen, "Generic multiuser coordinated beamforming for underlay spectrum sharing," *IEEE Transactions on Communications*, vol. 64, no. 6, pp. 2285–2298, May 2016.

[15] F. A. Khan, K. Tourki, M. Alouini, and K. A. Qaraqe, "Performance analysis of a power limited spectrum sharing system with TAS/MRC," *IEEE Transactions on Signal Processing*, vol. 62, no. 4, pp. 954–967, Jan. 2014.

[16] M. Hanif, H. Yang, and M. Alouini, "Transmit antenna selection for power adaptive underlay cognitive radio with instantaneous interference constraint," *IEEE Transactions on Communications*, vol. 65, no. 6, pp. 2357–2367, Mar. 2017.

[17] R. Sarvendranath and N. B. Mehta, "Exploiting power adaptation with transmit antenna selection for interference-outage constrained underlay spectrum sharing," *IEEE Transactions on Communications*, vol. 68, no. 1, pp. 480–492, Oct. 2020.

[18] R. M. Rao, H. S. Dhillon, V. Marojevic, and J. H. Reed, "Analysis of worst-case interference in underlay radar-massive MIMO spectrum sharing scenarios," in *IEEE Global Communications Conference (GLOBECOM)*, HI, USA, Feb. 2019, pp. 1–6.

[19] S. Dadallage, C. Yi, and J. Cai, "Joint beamforming, power, and channel allocation in multiuser and multichannel underlay MISO cognitive radio networks," *IEEE Transactions on Vehicular Technology*, vol. 65, no. 5, pp. 3349–3359, June 2016.

[20] S. Kusaladharma and C. Tellambura, "Secondary user interference characterization for spatially random underlay networks with massive MIMO and power control," *IEEE Transactions on Vehicular Technology*, vol. 66, no. 9, pp. 7897–7912, Sep. 2017.

[21] V. Nguyen, L. Tran, T. Q. Duong, O. Shin, and R. Farrell, "An efficient precoder design for multiuser MIMO cognitive radio networks with interference constraints," *IEEE Transactions on Vehicular Technology*, vol. 66, no. 5, pp. 3991–4004, May 2017.

[22] S. Kashyap and N. B. Mehta, "SEP-Optimal transmit power policy for peak power and interference outage probability constrained underlay cognitive radios," *IEEE Transactions on Wireless Communications*, vol. 12, no. 12, pp. 6371–6381, Dec. 2013.

[23] A. Ghasemi and E. S. Sousa, "Fundamental limits of spectrum-sharing in fading environments," *IEEE Transactions on Wireless Communications*, vol. 6, no. 2, pp. 649–658, Feb. 2007.

[24] K. Zheng, X. Liu, X. Liu, and Y. Zhu, "Hybrid overlay-underlay cognitive radio networks with energy harvesting," *IEEE Transactions on Communications*, vol. 67, no. 7, pp. 4669–4682, Apr. 2019.

[25] P. K. Sangdeh, H. Pirayesh, A. Quadri, and H. Zeng, "A practical spectrum sharing scheme for cognitive radio networks: Design and experiments," *IEEE/ACM Transactions on Networking*, vol. 28, no. 4, pp. 1818–1831, Aug. 2020.

[26] D. Tse and P. Viswanath, *Fundamentals of Wireless Communication*. USA: Cambridge University Press, 2005.

[27] S. N. Affes, H. Hansen, and P. Mermelstein, "Interference subspace rejection: a framework for multiuser detection in wideband CDMA," *IEEE Journal on Selected Areas in Communications*, vol. 20, no. 2, pp. 287–302, Aug. 2002.

[28] U. Madhow, "Blind adaptive interference suppression for direct-sequence CDMA," *Proceedings of the IEEE*, vol. 86, no. 10, pp. 2049–2069, Oct. 1998.

[29] H. Hotelling, "Relations between two sets of variates," *Biometrika*, vol. 28, no. 3/4, pp. 321–377, 1936.

[30] M. S. Ibrahim and N. Sidiropoulos, "Cell-edge interferometry: Reliable detection of unknown cell-edge users via canonical correlation analysis," in *IEEE Int. Conf. on Sig. Proc. Adv. in Wir. Comm. (SPAWC)*, Cannes, France, July 2019, pp. 1–5.

[31] Q. Wu and K. M. Wong, "Un-music and un-cle: An application of generalized correlation analysis to the estimation of the direction of arrival of signals in unknown correlated noise," *IEEE Transactions on Signal Processing*, vol. 42, no. 9, pp. 2331–2343, Sep. 1994.

[32] A. Dogandzic and A. Nehorai, "Finite-length MIMO equalization using canonical correlation analysis," *IEEE Transactions on Signal Processing*, vol. 50, no. 4, pp. 984–989, Aug. 2002.

[33] Z. Bai, G. Huang, and L. Yang, "A radar anti-jamming technology based on canonical correlation analysis," in *International Conference on Neural Networks and Brain*, vol. 1, Beijing, China, Apr. 2005, pp. 9–12.

[34] M. S. Ibrahim and N. D. Sidiropoulos, "Weak target detection in MIMO radar via beamspace canonical correlation," in *IEEE 11th Sensor Array and Multichannel Signal Processing Workshop (SAM)*, Hangzhou, China, June 2020, pp. 1–5.

[35] A. Bertrand and M. Moonen, "Distributed canonical correlation analysis in wireless sensor networks with application to distributed blind source separation," *IEEE Transactions on Signal Processing*, vol. 63, no. 18, pp. 4800–4813, June 2015.

[36] M. Borga and H. Knutsson, "A canonical correlation approach to blind source separation," *Report LiU-IMT-EX-0062 Department of Biomedical Engineering, Linkping University*, 2001.

[37] M. S. Ibrahim and N. D. Sidiropoulos, "Reliable detection of unknown cell-edge users via canonical correlation analysis," *IEEE Transactions on Wireless Communications*, vol. 19, no. 6, pp. 4170–4182, Mar. 2020.

[38] M. S. Ibrahim, A. S. Zamzam, A. Konar, and N. D. Sidiropoulos, "Cell-edge detection via selective cooperation and generalized canonical correlation," *IEEE Transactions on Wireless Communications*, May 2021.

[39] R. Arora and K. Livescu, "Multi-view learning with supervision for transformed bottleneck features," in *IEEE International Conference on Acoustics, Speech and Signal Processing (ICASSP)*, Florence, Italy, May 2014, pp. 2499–2503.

[40] X. Fu, K. Huang, E. Papalexais, H. A. Song, P. P. Talukdar, C. Faloutsos, N. D. Sidiropoulos, and T. Mitchell, "Efficient and distributed generalized canonical correlation analysis for big multiview data," *IEEE Transactions on Knowledge and Data Engineering*, pp. 1–1, Oct. 2018.

[41] C. I. Kanatsoulis, X. Fu, N. D. Sidiropoulos, and M. Hong, "Structured sumcor multiview canonical correlation analysis for large-scale data," *IEEE Transactions on Signal Processing*, vol. 67, no. 2, pp. 306–319, Jan. 2019.

[42] D. R. Hardoon, S. Szedmak, and J. Shawe-Taylor, "Canonical correlation analysis: An overview with application to learning methods," *Neural Computation*, vol. 16, no. 12, pp. 2639–2664, Dec. 2004.

[43] J. D. Carroll, "Generalization of canonical correlation analysis to three or more sets of variables," in *Proceedings of the 76th annual convention of the American Psychological Association*, vol. 3, 1968, pp. 227–228.

[44] C.-A. Deledalle, L. Denis, S. Tabti, and F. Tupin, "Closed-form expressions of the eigen decomposition of 2 x 2 and 3 x 3 hermitian matrices," Ph.D. dissertation, Université de Lyon, 2017.

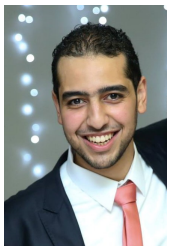

**Mohamed Salah Ibrahim** (Member, IEEE) received the B.Sc. degree (Hons.) in electrical engineering from Alexandria University, Alexandria, Egypt, in 2013, the M.Sc. degree in wireless technologies from Nile University, Giza, Egypt, in 2016, and the Ph.D. degree in electrical engineering from the University of Virginia, Charlottesville, VA, USA, in 2021. He is currently a senior engineer in the Research and Innovation Department in InterDigital Communications, Conshohocken, PA, USA. His research interests include wireless communications, signal processing, optimization, and machine learning. He was a finalist of the Best Student Paper Competition at IEEE SPAWC 2018. He has held R&D internships with FutureWei Technologies (Huawei), Chicago, IL, and Nokia Bell Labs, Murray Hill, NJ. He has received the Louis T. Rader Graduate Research Award from the University of Virginia in 2021.

**Paris A. Karakasis** (Student Member, IEEE) received the Diploma and M.Sc. degree in Electrical and Computer Engineering from the Technical University of Crete, Chania, Greece, in 2017 and 2019, respectively. Since January 2020, he has been a Ph.D. student at the Electrical and Computer Engineering Department, University of Virginia, Charlottesville, VA, USA. His research interests include signal processing, numerical optimization, machine learning, tensor decomposition, and graph mining.

**Nicholas D. Sidiropoulos** (Fellow, IEEE) received the Diploma in electrical engineering from the Aristotle University of Thessaloniki, Thessaloniki, Greece, and the M.S. and Ph.D. degrees in electrical engineering from the University of Maryland at College Park, College Park, MD, USA, in 1988, 1990, and 1992, respectively. He is the Louis T. Rader Professor at the University of Virginia. He has previously served on the faculty of the University of Minnesota, and the Technical University of Crete, Greece. His research interests are in signal processing, communications, optimization, tensor decomposition, and factor analysis, with applications in machine learning and communications. He received the NSF/CAREER award in 1998, and the IEEE Signal Processing Society (SPS) Best Paper Award in 2001, 2007, and 2011. He served as IEEE SPS Distinguished Lecturer (2008–2009), as Vice President - Membership of IEEE SPS (2017–2019), and as chair of the SPS IEEE Fellow Evaluation Committee (2020-2021). He received the IEEE Signal Processing Society Meritorious Service Award (2010), the Distinguished Alumni Award of the Department of ECE, University of Maryland (2013), and the EURASIP Technical Achievement Award (2022). He is a Fellow of EURASIP (2014).